WATER RESOURCES RESEARCH, VOL. 31, NO. 12, PAGES 2927–2943, DECEMBER 1995

Computer construction of fractal soil structures: Simulation of their hydraulic and shrinkage properties

Edith Perrier, Christian Mullon, and Michel Rieu
Laboratoire d'Informatique Appliquée, Laboratoire d'Hydrophysique, Bondy, France

Ghislain de Marsily
Laboratoire de Géologie Appliquée, Université Pierre et Marie Curie, Paris, France

Abstract. To study relationships between soil hydraulic properties and soil structural properties, a computer micro model of soil is constructed. We present first a general method of building a two-dimensional porous structure, including both pores and particles, with different levels of aggregation resulting from a fragmentation process. A fractal structure is obtained when self similarity is imposed over the successive scales of fragmentation. Emphasis is put upon the modeling of the retention curve. A classical capillary model and methods taken from percolation theory enable us to simulate qualitatively the primary and secondary loops of this hysteretic curve. In the fractal case, theoretical analytical expressions proposed for adjusting retention data are tested. The unsaturated hydraulic conductivity is also calculated on the same simulated soil by analogy with an electrical network. The soil structures are deformable and simulation proves to be a useful tool to investigate the behavior of swelling soils.

Introduction

Knowledge of the specific hydraulic behavior of a given soil is needed to model water transport in the unsaturated zone. The basic hydraulic properties, mainly the retention and conductivity curves, are usually determined by controlled flow experiments either in the laboratory or in the field. It is an old dream among soil scientists to directly relate these hydraulic properties to structural properties which could be obtained more easily on dry soil samples. Numerous attempts have been made to find either statistical relations or deterministic links between structural data and hydraulic properties. This paper is concerned with a deterministic approach.

Research has been done [e.g., *Arya and Paris*, 1981; *Haverkampf and Parlange*, 1986; *Tyler and Wheatcraft*, 1989, 1992] to link hydraulic properties to the particle size distribution in a soil, which structural information is easily and widely obtained through mechanical sieving. The texture models whose definition of the soil is based on matrix properties such as particle diameter or particle shape (e.g., the spheres models) view the solid phase as a set of discrete particles and the void phase as a continuum. The complex geometry of the remaining voids makes the analysis of flow too difficult unless one works at the Navier-Stokes scale, dealing with only a few particles as in lattice gas simulations [*di Pietro et al.*, 1994]. At the pore scale, the pore space must be divided into a set of simple geometric parts, such as cylinders or parallepipeds, so that integrated forms of the fluid movement equations can be used. A common approach is therefore to invent a pore space model with a simple geometry that can be associated with the particle distribution. For example, *Arya and Paris* [1981] associated a tube with each particle size class and treated the pore space as a bundle of capillary tubes. However, to obtain good agreement between calculated and observed retention data, they needed to add an empirical fitting parameter. It is clear that water flows through the voids of the soil, and that transport properties are determined by the pore geometry. Thus the aim is to discover how pore distribution can be related to a given particle distribution.

Other authors have considered the solid phase as a continuum, cut through by a set of discrete pores: their modeling approach is based directly on the pore size distribution, using capillary models. To predict retention and conductivity curves, some of them simply associated a bundle of tubes with distinct pore size classes [e.g., *Marshall*, 1958] or worked with continuous pore size distribution density function [*Mualem*, 1974, 1976], while others [*Thirriot*, 1981; *Billotte*, 1986] delt with interconnected tubes in a probabilistic manner. The use of computers has made it possible to simulate soil porosity by a network of tubes which represents real porous media more accurately [*Fatt*, 1956] by accounting for the topology of the pore space. Subsequently, considerable work has been done on pore or fracture networks [*Chatzis and Dullien*, 1977, 1982; *Thirriot*, 1982; *Wilkinson*, 1984, 1986; *Charlaix*, 1987; *Diaz et al.*, 1987; *Lenormand et al.*, 1988; *Billaux*, 1990; *Cacas et al.*, 1990a,b; *Daian and Saliba*, 1991; *Martys et al.*, 1991; *Wise*, 1992; *Koiller and Robbins*, 1992; *Blunt et al.*, 1992; *Nordqvist et al.*, 1992; *Ewing and Gupta*, 1993a,b] within the general framework of the theory of percolation in disordered networks.

In any event, if we want to use a network model on real soil, we have to know what pore size distribution to enter into the model. The distribution calculated from image analysis is not entirely reliable due to the two-dimensional approach, and that obtained from mercury porosimetry measurements often results from the assumptions made in the oversimplified bundle of tubes. Moreover, these data mainly consist of estimates of the pore size distribution in a dry soil sample. However, many soils are more or less deformable and even without any mechanical constraints the particle packing changes with moisture

Copyright 1995 by the American Geophysical Union.

Paper number 95WR02214.

ORSTOM Documentation
010004079
Fonds Documentaire ORSTOM
Cote: B* 4079 Ex: 1

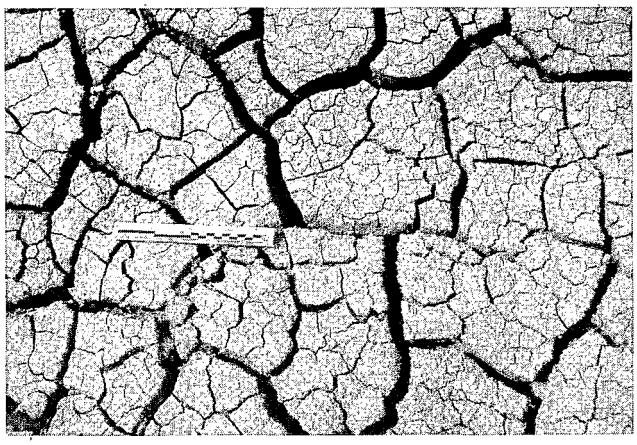

Figure 1. The surface of a drying vertic soil (photograph from North Senegal).

content: the pore network evolves, while the particle distribution remains unchanged. Deformability is usually neglected in standard modeling but our belief is, on the contrary, that a better knowledge of the structural organization of the soil can be deduced from precise deformability measurements. It is, therefore, important to discover how the effective pore size distribution can be reliably assessed.

Construction of Soil Structures

This study is based on a new approach in computer science, which uses the concept of "virtual reality." Instead of working on conceptual models of soils to reproduce soil hydraulic properties, we looked for simple rules of construction of virtual soil samples presenting structural properties analogous to the real ones, then explore, by simulation, their hydraulic properties to compare them with reality and discuss the assumptions made.

Real soil structures can be defined as complex geometric arrangements of elementary structural units, particles, and pores: a porous structure is built here as a discontinuous set of both solid and void elements, whose two main characteristics are a particle size distribution (PSD) and a pore size distribution (psd). Real soils, and particularly aggregated soils, have often been described as porous media structured on different organization scales [e.g., *Oades and Warters*, 1991]; for example, several authors [*Othmer et al.*, 1991; *Gerke and van Genuchten*, 1992] have worked on soils presenting only "a dual porosity" on two levels, whereas observations of the surface of a drying vertic soil reveal several embedded levels of aggregation (see Figure 1). Therefore our model can represent particle packings in soil aggregates on successive hierarchical levels. Particular attention is focused on the behavior of swelling soils where shrinking and swelling phenomena occur with variations in moisture content. Deformable convex areas representing aggregates of particles are designed to handle isotropic deformations.

All the elementary structural units are represented by individualized computer objects. Simulating their interdependence in a whole geometric structure is made easier by an "object-oriented" programming style. The work is done in two dimensions: surfaces represent volumes and are extrapolated to three dimensions under very simple assumptions when numerical results are needed.

Construction on One Level of Fragmentation

The sample of studied soil is represented by a polygon P_0 (mainly a square). A fragmentation process is simulated: a set of initial points (fragmentation seeds) is generated inside P_0 (Figure 2a). Then a space partition is made in order to split P_0 into polygonal zones surrounding each point: the polygon $P(M)$ associated with a point M is the set of points whose nearest seed point is M (Figure 2a). The algorithm is called a Voronoï tesselation (or a Dirichlet tesselation, e.g., *Green and Sibson* [1977], or the so-called determination of the Theissen polygons in hydrology) and consists of a rather complicated determination of successive perpendicular bisectors between two neighboring points. An irregular grid is obtained which is called the invariant skeleton of the structure (Figure 2b). Any initial set of points can be used. The "random" case reported in this paper refers to a set of points generated with uniformly distributed coordinates (Figure 2a).

A porous structure (Figure 2c) is then created by means of a homothetic reduction $\mathcal{H}(G, k)$ of each initiating zone P. G is the center of gravity of the convex polygon P and k can be chosen to generate a given total porosity. The reduced polygon

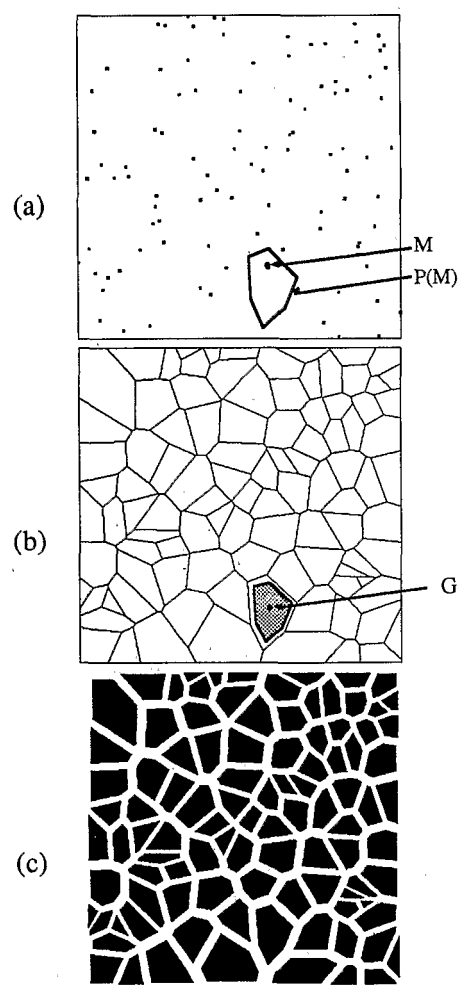

Figure 2. Construction of a soil structure on one level of fragmentation (a) 100 Poisson points chosen as random fragmentation seeds, (b) fragmentation zones associated by a Voronoï tessellation, and (c) pores and solid elements created by homothetically reducing each fragmentation zone about its gravity center with a constant ratio ($k = 0.8$).

represents a solid element; the opening between two solids represents a pore. (At this stage, the method is quite similar to the "grain boundary model" of *Winterfeld* [1981], who presented an indepth study of the electrical conductivity of such models, when both solid rock elements and cracks may be conductors).

When the same k value is attributed to each polygon P, the PSD is proportional to the initial distribution of the polygonal zones and is entirely determined by the choice of the initial points. One single psd is associated with the PSD. An undeformable porous structure is defined by a skeleton and a homothetic ratio k. One component of the model is an irregular pore network which results from the geometrical constraints imposed by the space partitioning into either solid or void.

Construction on Several Levels of Fragmentation

The process described above can be repeated on successive levels of fragmentation. What we have so far called solid elements will now represent microporous aggregates that are divided into smaller aggregates or particles. Once a set of points has been generated in the initial zone P_0 which fragmented into N_1 smaller zones $P_{1j}(1 \leq j \leq N_1$, Figure 3a), a new set of points is generated within each zone P_{1j} which determines a partitioning of each P_{1j} into N_2 smaller zones $P_{2j}(1 \leq j \leq N_1N_2$ at level 2, Figure 3b) and so on up to the ultimate level n of fragmentation ($\Pi_{i=1}^{n} N_i$ zones at level n, Figure 4a) to define a new type of structure skeleton. Embedded aggregates of particles and pores are created in the same way: at each level i, a homothetic transformation $\mathcal{H}(G_{ij}, k_i)$ is applied on each zone P_{ij} with a given ratio k_i from the center of gravity G_{ij} of P_{ij} to create an aggregate A_{ij} (Figures 3c and 3d). At the last level n, A_{nj} represents a solid particle. The number N_i of subaggregates and the k_i reduction ratio can be given any relevant values. A rigid porous structure is defined by a skeleton and a set $(k_1, k_2, \cdots k_i, \cdots, k_n)$ of homothetic ratios, where the subscript i refers to the fragmentation level.

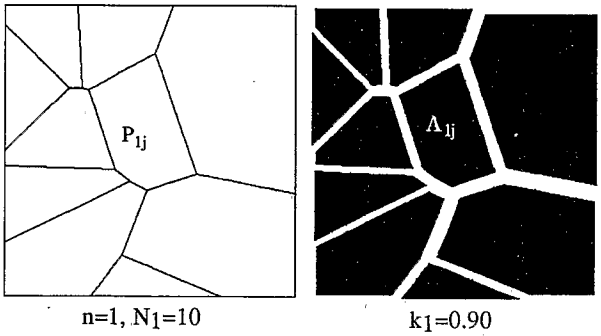

n=1, N1=10 k1=0.90

(a) surf(A1j)=k1²surf(P1j)

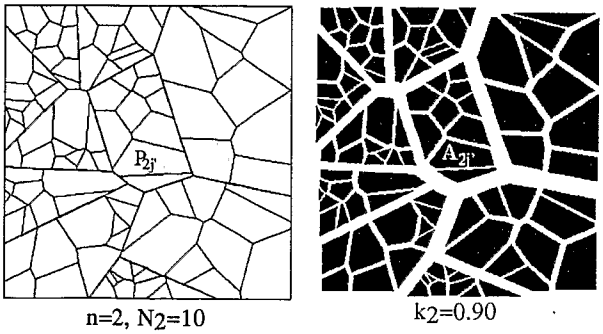

n=2, N2=10 k2=0.90

(b) surf(A2j')=k1²k2²surf(P2j')

Figure 3. Construction of a soil structure on several levels of fragmentation (a) first level and (b) second level.

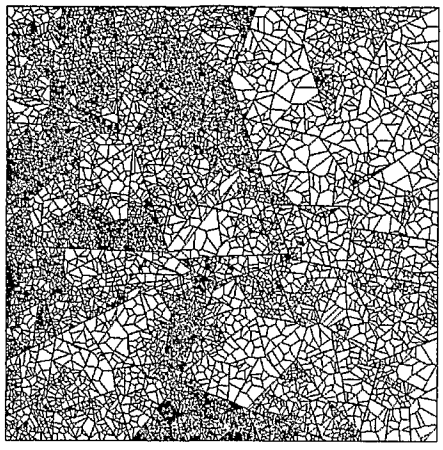

(a) n=4, N1=N2=N3=N4=10

(10^4 fragmentation zones at last level 4)

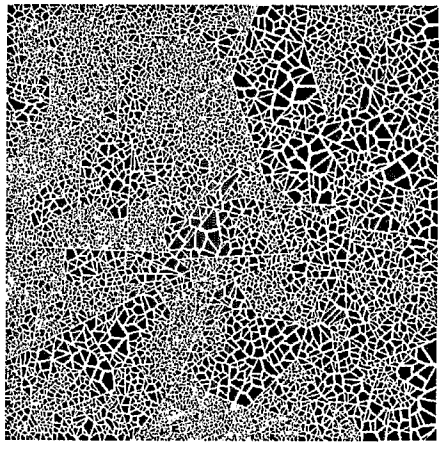

(b) k1=k2=k3=1, k4=0.85 (k0=1)

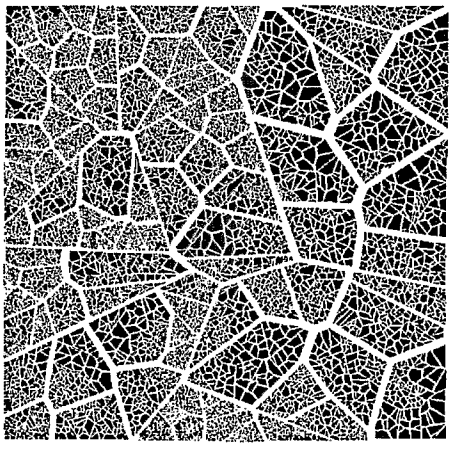

(c) k1=1, k2=0.92, k3=1, k4=0.92 (k0=1)

Figure 4. Different soil structures associated with the same particle size distribution (PSD), same total porosity and different pore size distribution (psd): (a) structure skeleton, (b) first example of associated structure with no visible aggregates, and (c) second example of structure with a homothetic ratio $k2 \neq 1$ defining aggregates of particles at level 2.

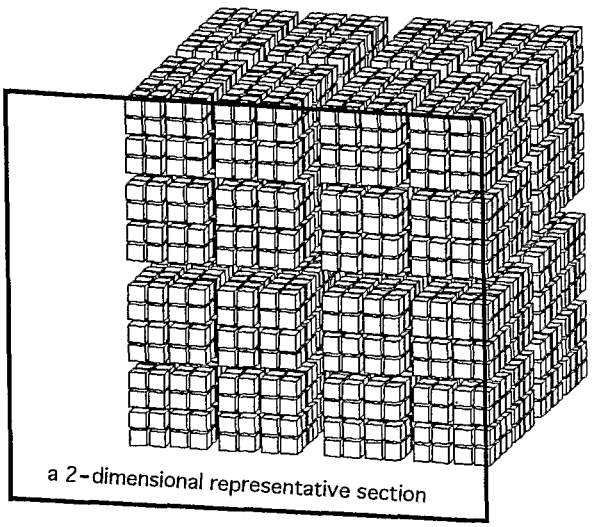

Figure 5. Illustration of the fractal model adapted from *Rieu and Sposito* [1991a].

Different models of soil structures corresponding to different types of soil aggregations can be associated with the same skeleton (Figure 4). Different clustering patterns are simulated with a packing ($k_i < 1$) or nonpacking ($k_i = 1$) process into aggregates of level i. They lead to different psd that may fit the same total porosity and the same PSD as in Figures 4b and 4c.

Fractal Structures

Fractal geometry appears to be useful for describing many porous media [*Pfeifer and Avnir*, 1983; *de Gennes*, 1985; *Katz and Thompson*, 1985; *Jullien and Botet*, 1986; *Friesen and Mikula*, 1987; *Delannay et al.*, 1989] and particularly soil structures [*Tyler and Wheatcraft*, 1989, 1990, 1992; *Ahl and Niemeyer*, 1989a, b; *Toledo et al.*, 1990; *Bartoli et al.*, 1991; *Young and Crawford*, 1991; *Rieu and Sposito*, 1991a, b; *Ghilardi et al.*, 1993]. *Rieu and Sposito* [1991a, b] have described the observed similarity in different organization levels of structured soils by means of a fractal model (Figure 5). In our construction, self similarity can be produced (on average) by a constant number N of subaggregates "daughters" and the same homothetic ratio k for all the homothetic transformations on any aggregate at any level. The simulated porous structure (e.g., Figure 6) is then a statistical realization of the theoretical fractal fragmented porous media proposed by these authors. According to the definition of the fractal dimension $\mathfrak{D}$ from the self similarity of a set of objects, $\mathfrak{D} = -\log n/\log r$, where each object of linear size $\mathcal{L}$ generates n similar objects of linear size $r\mathcal{L}$ when the resolution scale is increased. In the two-dimensional computer realization, each zone P_{ij} of linear size $\mathcal{L}(P_{ij})$ is divided into N subzones of mean linear size $\mathcal{L}(P_{ij})/N^{1/2}$. After the homothetic transformation of ratio k, each aggregate is divided into N similar subaggregates of mean linear size reduced by $k/N^{1/2}$ thus $n = N$, $r = k/N^{1/2}$, and $\mathfrak{D}_2 = -\log n/\log r = 2 \log N/(\log N - 2 \log k)$. Assuming isotropy, the N polygonal zones represented in two dimensions correspond to $n = N^{3/2}$ polyhedral zones in a three-dimensional associated structure where homothetic transformations lead to the same ratio r between successive linear sizes. Thus in three dimensions, $n = N^{3/2}$, $r = k/N^{1/2}$, and the fractal dimension is $\mathfrak{D}_3 = 3 \log N/(\log N - 2 \log k) = 3/2(\mathfrak{D}_2)$. Figure 6 shows an example where $\mathfrak{D}_3 \cong 2.897$ ($N = 10$, $k = 0.96$) and the fractal psd is developed around the same particles and with the same total porosity as in Figure 4. The two-dimensional image is not random but a representative section of planar pores that we assume to be cut through by similar planar pores in the third dimension (see Figure 5).

Deformability

This method of structure building has been imagined to permit the simulation of dynamic deformations. Figures 4b and 4c depict two types of aggregation in different soils. They can also represent two stages of aggregation in the same soil at two distinct swelling states. For example, Figure 4b could represent the opening of a wet soil structure while Figure 4c could represent the cracks after a drying process in a swelling soil.

Remember that a rigid porous structure has been defined by a skeleton (an initial zone P_0 partitioned in polygonal zones P_{ij} at each level of fragmentation i) and by a set $\{k_i\}_{i=1 \dots n}$ of homothetic ratios. A swelling state (s) of a deformable porous structure is now defined by an invariant skeleton and a set $\{k_{i(s)}\}_{i=0 \dots n}$ of variable homothetic ratios. In the case of a rigid structure, the parameter k_0 was not mentioned and was set to 1. It can now take different values in swelling or shrinking soils. All the pore, particle, or aggregate surfaces are measured on the simulated soil structure and normalized by the invariant surface surf(P_0) of the reference zone P_0 (surf(P_0) set equal to 1). The whole soil sample is defined by the homothetic transformation of P_0 with a ratio k_0, its surface is $S_0(s) = k_0(s)^2\text{surf}(P_0) = k_0(s)^2$ and represents the macroscopic soil volume whose changes are simulated by variations of $k_0(s)$.

The volumes of the aggregates vary during a deformation process and can also be calculated from the represented surfaces. For a given swelling state (s) of the structure, the ag-

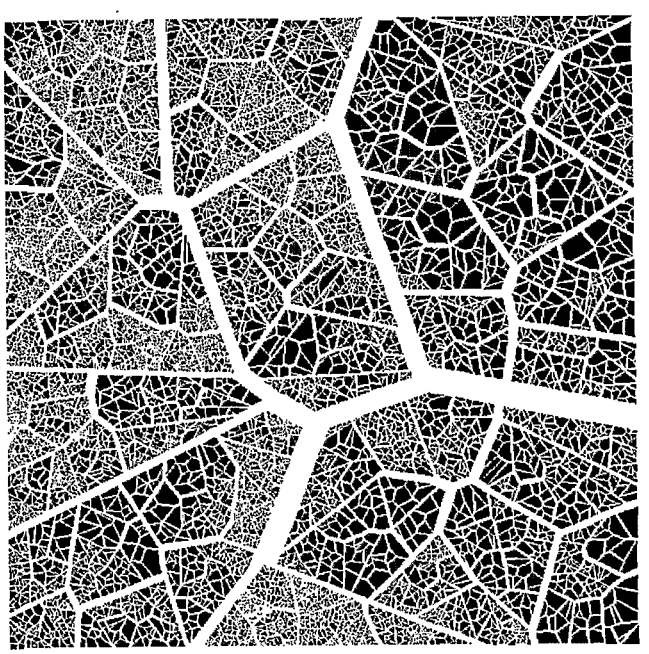

n=4, N=10; k=0.96, D_{def}=2.898

Figure 6. A fractal structure associated with the structure skeleton shown on Figure 4a, presenting the same particle distribution (PSD) and the same total porosity as structures shown on Figure 4b and 4c.

gregate A_{ij} associated with any zone P_{ij} is a homothetic replica of P_{ij}, and its surface is $(k_0(s)k_1(s) \cdots k_i(s))^2$ times the initial surface (P_{ij}) (see Figure 3). Let us call $S_i(s)$ the partial surface occupied by all the aggregates of level i and denote $\lambda_i(s) = \Pi_{j=0}^{i} (k_j(s))$ for greater readability.

$$S_i(s) = \sum_j \text{surf}\,(A_{ij}) = \sum_j \lambda_i(s)^2 \,\text{surf}\,(P_{ij})$$

$$= \lambda_i(s)^2 \sum_j \text{surf}\,(P_{ij}) = \lambda_i(s)^2 \,\text{surf}\,(P_0),$$

since at each level i, the set of polygonal zones P_{ij} is a partition of P_0. Thus $S_i(s)$ is determined by the value of the product of the successive homothetic ratios:

$$S_i(s) = \prod_{j=0}^{i} (k_j(s))^2 \tag{1}$$

In the extrapolation to the third dimension, as explained before, the planar reference zone P_0 is associated with a three-dimensional zone partitioned into a set of polyhedral zones, and the same reasoning leads to the following expression for the partial volume $V_i(s)$ occupied by all the aggregates of level i:

$$V_i(s) = \prod_{j=0}^{i} (k_j(s))^3 \tag{2}$$

The only condition for realistic deformation is that the particles remain unchanged, thus the total surface $S_n(s)$ of the particles at the last level of fragmentation n, representing the volume $V_n(s)$ of the solid phase, must be constant: $\Pi_{i=0}^{n} (k_i(s))$ must be independent of s. At other levels i, $S_i(s)$ (or $V_i(s)$) can have any value as long as aggregates do not overlap, which is verified empirically by summing up the pores and particle surfaces at each moment and comparing them to the total surface of the sample. Hence for the same PSD, many different swelling states of the structure can be simulated.

Simulation of the Retention Curve

Reference Retention Curve Associated to a Pore Size Distribution

A first component of the structure is a set of simple pores which in this model are channels representing sections of three-dimensional fractures. A simple capillary model is used in interpreting the distribution of two nonmiscible fluids in a porous medium (the wetting fluid is water, while the nonwetting fluid is air), assuming Laplace's law to be valid throughout the pore distribution range in the following simplified manner. For a given capillary pressure h and the corresponding equilibrium state, a pore p is filled with water (or air) if its aperture is smaller than $r = \gamma/h$ (or larger than $r = \gamma/h$) (condition 1), where γ is a constant that could be calculated from the liquid-solid contact angle and the liquid-water-air surface tension.

It is then easy to calculate a moisture content related to any capillary pressure h by means of the pore distribution. At any given capillary pressure h, the water content θ is equal to the sum of the volumes of all the pores with an aperture smaller than r. The pore volume is calculated from the pore surface as explained in the appendix. The capillary retention curve thus

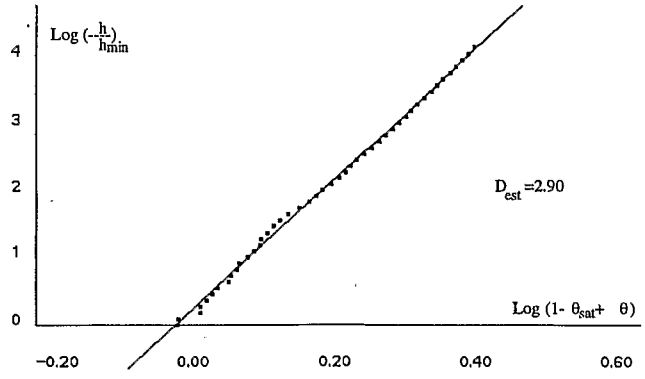

(a) adjustment of expression (3)

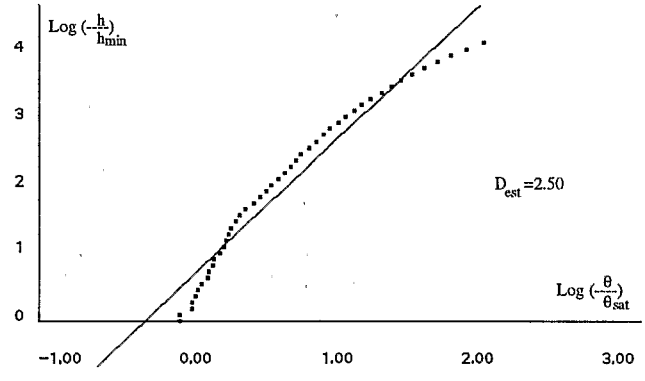

(b) adjustment of expression (4)

Figure 7. Adjustment of the reference retention curve calculated on the fractal structure shown in Figure 6 to theoretical analytical (3) and (4).

obtained is called "reference curve" (see Figure 9 and Figure 11a).

Calculation of the Retention Curve in Fractal Structures

Two theoretical analytical expressions have been proposed for modeling the pressure water content (h, θ) relation in fractal soils. A first expression was established by *Rieu and Sposito* [1991]:

$$\theta(h) = (h/h_{\min})^{D-3} + \theta_{\text{sat}} - 1, \tag{3}$$

where θ is water content, h is capillary pressure, θ_{sat} is water content at saturation, $h_{\min}$ is air entry pressure, and D is fractal dimension.

Other authors [*Tyler and Wheatcraft*, 1990; *Toledo et al.*, 1990] have also worked on a fractal soil model of dimension D' and derived another analytical expression:

$$\theta(h)/\theta_{\text{sat}} = (h/h_{\min})^{D'-3} \tag{4}$$

This expression was first established by *Brooks and Corey* [1964] who simply considered $D' - 3$ as an empirical exponent.

Here (3) is used to determine the fractal dimension D from the slope of the regression line fitted by a plot of log $(h/h_{\min})$ versus log $(1 - \theta_{\text{sat}} + \theta)$, while (4) is used to determine the fractal dimension D' from the slope of the regression line fitted by the plot of log $(h/h_{\min})$ versus log $(\theta/\theta_{\text{sat}})$. We tested these two methods on the drainage retention curve simulated on our fractal soil structures.

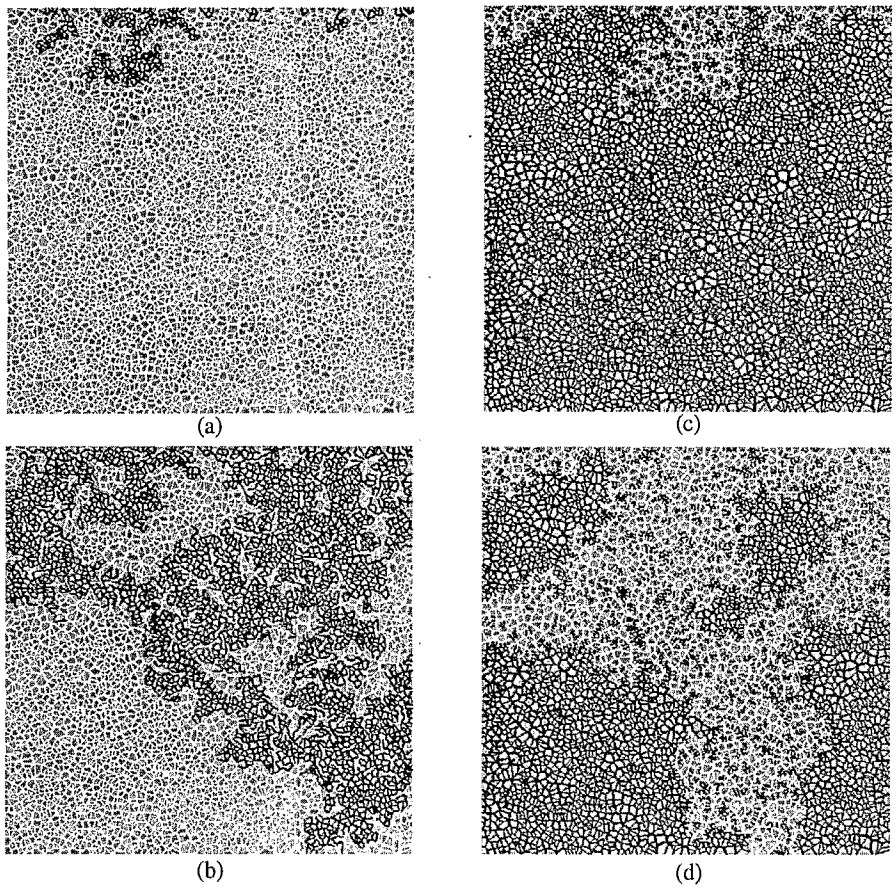

Figure 8. Invasion percolation on a random structure (5000 particles, $k = 0.80$). Figure 8a and 8b is invasion of water into a dry soil and Figure 8c and 8d is invasion of air into a water-saturated soil.

Let us consider a soil structure generated with a given fractal dimension D_{def} (Figure 6). The estimation D_{est} of D from the adjustment of the calculated retention curve to (3) (Figure 7a) is almost exactly equal to D_{def} (on 300 random simulations where $2 < D_{\text{def}} < 3$, $n > 2$, with 50 simulated points (θ, h), the mean squared correlation coefficient is $R^2 = 0.99$, and the mean deviation $|D_{\text{est}} - D_{\text{def}}|$ is 0.005), which confirms that we succeeded in constructing a statistical realization of the deterministic theoretical fractal model which was illustrated in *Rieu and Sposito* [1991a] by cubic particles of a single size. The retention curve does not depend on the number n of fragmentation levels but only on the total porosity and on the fractal dimension.

The adjustment to (4) shows a strong deviation from linearity (see Figure 7b) and moreover, it leads to a value of D'_{est} smaller than D_{def}. We thus show that the two analytic expressions are definitively not equivalent because they lead to quite different fractal values D and D' on the same simulated data. This obvious difference can be explained [*Perrier*, 1994] as follows: Here (4) is derived on a fractal psd entirely developed toward infinitely small pore sizes, whereas (3) assumes a lower scale cutoff for the same psd. Also, (4) has not yet been associated with a complete fractal model of soil structure made of both solids and voids. Such a model exists, but it must be different from the fractal model of aggregated soils presented here, where an infinite development would lead to the disappearance of the solid phase (note that in this case, θ_{sat} would tend toward 1, (4) and (3) would then become equivalent). This question will be fully addressed in a forthcoming paper.

Simulation of Air or Water Invasion in a Pore Network

A second component of the structure is the topology of the pore network. The simulation of the invasion by a fluid of an interconnected pore network introduces a new idea: the invading fluid can only penetrate a pore if it is accessible, that is, connected to the supply faces. A connectivity condition is added to condition 1: A pore p may be filled with water (or air) if it is connected to the supply face through a continuous path of water (or air) (condition 2). For example, consider a square sample of entirely dry porous medium and assume that water is introduced at the upper edge. Successive pressure equilibrium states are then simulated, assuming very slow moves from one state to the other, so as to allow capillary forces to dominate. For high capillary pressure, water will first penetrate the narrowest pores but only if they are connected to the upper edge through a continuous supply path of water (Figure 8a). With a decrease in capillary pressure, the invading fluid gains access to larger pores and the medium is progressively filled with water (Figure 8b). The invasion of air into a medium initially saturated with water is simulated in the same way. Air flows first through the widest pores, then through narrower ones as the pressure increases (Figure 8c and 8d). So the modeling of fluid advance in the structure is based on the so-called "invasion percolation" process in a network, origi-

nated with *Wilkinson* [1984, 1986] and *Lenormand et al.* [1985]. In this study, the simplest assumptions have been made; namely, wetting and nonwetting fluids are treated symmetrically. Gravity effects, viscous forces, as well as trapping phenomena, are neglected.

Simulation of the Hysteresis of the Retention Curve

The very simple assumptions made in this first study appear to be strong enough to simulate the well-known hysteresis of the retention curve in any case. The retention curve is no longer strictly equivalent to a pore size distribution [*Zhou and Stenby*, 1993], and the simulated drainage and imbibition curves are located, respectively, above and below the calculated reference curve (Figure 9) as shown in comparable conditions by *Ewing and Gupta* [1993a,b].

The simulation of hysteretical retention curves has long been established on pore networks either in similar conditions [e.g., *Thirriot*, 1982] or using more sophisticated models. The extent of the hysteresis depends on the assumptions made both on the soil structure models and on the invasion principles. For example, it would increase if local correlations in the pore sizes were introduced by considering pore wide bodies linked by thinner throats, and it would decrease if weaker connectivity conditions were assumed in the imbibition phase [e.g., *Diaz et al.*, 1987; *Daian and Saliba*, 1991; *Blunt et al.*, 1992]. Namely, it has been shown [*Lenormand and Zarcone*, 1983] that while invasion by a nonwetting fluid seems well represented by an invasion percolation model, wetting invasion is ruled by much more complex rate-dependent mechanisms, including possible flow by water films along particles rough surface. Accounting for such physical mechanisms [e.g., *Blunt et al.*, 1992] would modify the shape of the imbibition curve presented in this paper.

The secondary hysteretic loops are similarly reproduced (Figure 10b) when the simulation is applied to a variably saturated initial medium (Figure 10a). The connectivity condition remains the same, but its application requires an improved algorithm. *Golden* [1980] showed that the phenomenon of secondary as well as primary hysteresis can be derived mathematically from percolation theory applied to simple pore network models, but we are not aware of any other systematic simulation of all possible secondary loops in the field of network modeling.

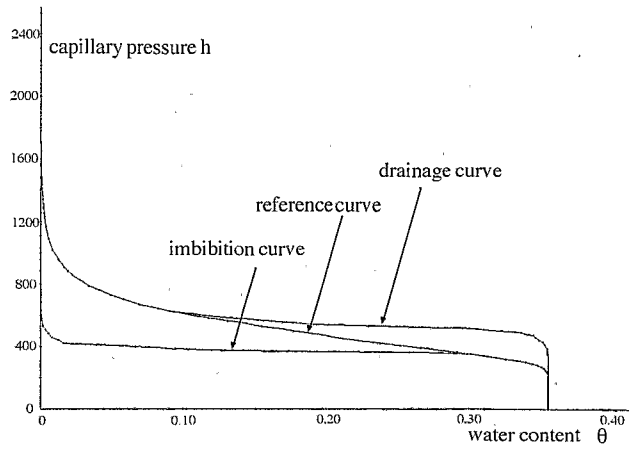

Figure 9. Hysteretical retention curve simulated on the random structure shown in Figure 8.

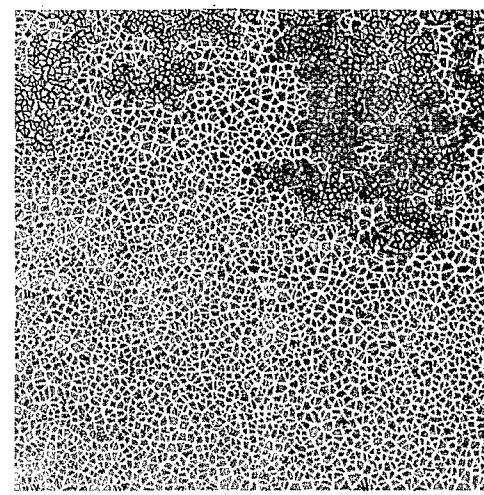

(a) water content θ(a), capillary pressure h(a)

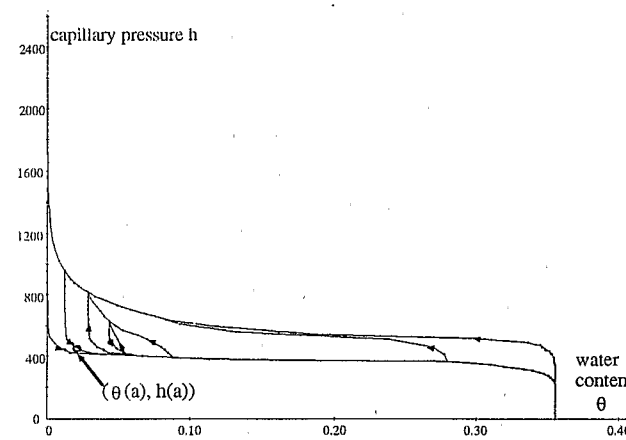

(b)

Figure 10. Simulation of secondary hysteresis of the retention curve: (a) invasion of water into a half-saturated medium and (b) simulation of several scanning loops of the curve shown in Figure 9.

In the fractal case, the simulated hysteresis is mainly due to the imbibition curve (Figure 11a). The spatial distribution of the pores in this construction implies that there is no constraint of accessibility during the drainage phase (Figure 11b) and a maximal constraint during the imbibition phase (Figure 11c). The consequences of the structuring of the medium are also felt in the shape of the invasion fronts (Figure 11b and 11c) which are very different from those obtained in the random case and classically obtained in disordered media (Figure 8). The previous results concerning the analytical expression of the retention curve in a fractal structure (when hysteresis was neglected) are kept only for the drainage curve.

Simulation of Deformation

Experimental Data and Swelling Soil Modeling

Soil deformation with variation in water content is mainly characterized by a shrinkage curve relating the bulk volume of a soil core to its specific water content [e.g., *Haines*, 1923; *MacGarry and Malafant*, 1987]. An experimental device was developed by *Braudeau* [1988a] to carry out on-line deforma-

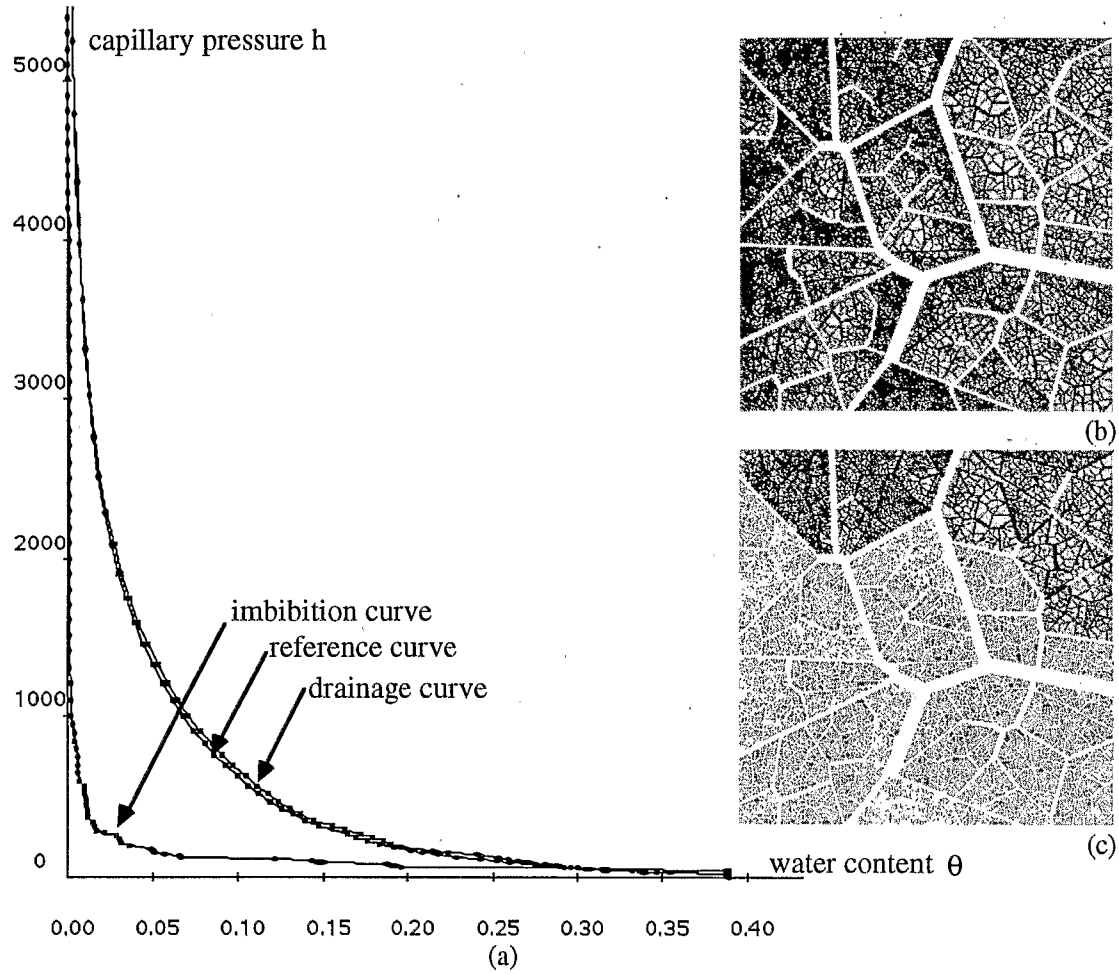

Figure 11. A fractal structure (same examples as in Figure 6). Simulated drainage and imbibition retention curves compared to (a) the reference curve and invasion fronts, respectively, in (b) drainage and (c) imbibition.

tion measurements on drying structured cylindrical soil cores. For each weighted water content, the vertical diameter of the core is measured. Assuming an isotropic deformation, the variation of the macroscopic volume is calculated. Thus a number of characteristic shrinkage curves (Figure 12a) are easily obtained [*Braudeau and Boivin*, 1995]. Different assumptions have been made to describe the shrinking behavior of a soil. For example, *Braudeau* [1988a,b] proposed a structure model for interpreting shrinkage curves. He defined a dual porosity in soils: the intraaggregate microporosity and the interaggregate macroporosity. From point C to the end of the drying (Figure 12a), the deformation would be entirely due to the microporosity of clayey aggregates whose elementary shrinking behavior follows that of pure clay [*Braudeau and Bruand*, 1993, Figure 12b]: they shrink and remain saturated with water up to point B where air begins to enter them. We will simulate different hypotheses to find what effects they have on the hydraulic properties of the soil.

Simulation Principle

Successive equilibrium capillary pressure states were again simulated. However, a variation in capillary pressure does not only imply a modification of the water content but also a possible variation in volume, which we extrapolate from two-dimensional simulations, assuming isotropy. The simulation works in alternate phases of deformation and redistribution of the fluids in the deformed structure. Each simulation step corresponds to a given pressure and is divided into two parts.

The first part consists in the geometrical deformation of the structure. At each step, a new swelling state (s') of the structure is calculated from the previous state (s). Remember that a swelling state (s) is defined by a list of ratios $(k_0(s), \cdots, k_i(s), \cdots, k_n(s))$ and corresponds to a given macroscopic volume $V_0(s)$ and partial volumes $V_i(s)$ of the aggregates at level i, where $V_i(s) = \Pi_{j=0}^{i} (k_j(s))^3$ (cf. (2)). If variations $(\Delta V_0, \cdots, \Delta V_i, \cdots, \Delta V_n)$ are imposed on the deforming structure, the new state vector after deformation $(k_0(s'), \cdots, k_{i(s')}, \cdots, k_n(s'))$ is easily calculated from the state vector $(k_0(s), \cdots, k_i(s), \cdots, k_n(s))$ before deformation:

$$\Delta V_i = \prod_{j=0}^{i} (k_j(s'))^3 - \prod_{j=0}^{i} (k_j(s))^3 \tag{5}$$

The calculation is done from top level 0 to bottom level n in a recurrent manner. First, if $i = 0$, $\Delta V_0 = (k_0(s'))^3 - (k_0(s))^3$ and $k_0(s')$ is calculated from $k_0(s)$ and ΔV_0. Then, at each level i, $k_i(s')$ is calculated from $\{k_j(s), j \leq i\}$, $\{k_j(s'), j < i\}$ and ΔV_i by rewriting (5) as follows:

$$k_i(s') = \left(\frac{\Delta V_i + \prod_{j=0}^{j=1} (k_j(s))^3}{\prod_{j=0}^{j=i-1} (k_j(s'))^3} \right)^{1/3}$$

The main assumption is that the filling state of each individual pore remains unchanged during the deformation phase. For example water-filled pores can be partly emptied of water due to their contraction and not to air entry according to Laplace's law.

The second part of the simulation consists in the redistribution of the liquid phase in the structure. The filling or emptying of those pores which fulfill both condition 1 and 2 is simulated as before.

Simulation Examples

Different deformation scenarios are created by choosing $(\Delta V_0, \cdots, \Delta V_i, \cdots, \Delta V_n)$ according to various assumptions and conditions. ΔV_0 expresses a measurable macroscopic volume change. If the last stage of fragmentation n represents the particle scale, as assumed until now, $\Delta V_n = 0$ (simulation 1). If n does not represent the actual last stage of fragmentation, but the last simulated state, the aggregates of the last level n represent microporous clayey aggregates whose volumes can vary (simulation 2). The following examples were simulated on the particular fractal structure shown in Figure 6, representing the initial swelling state at saturation.

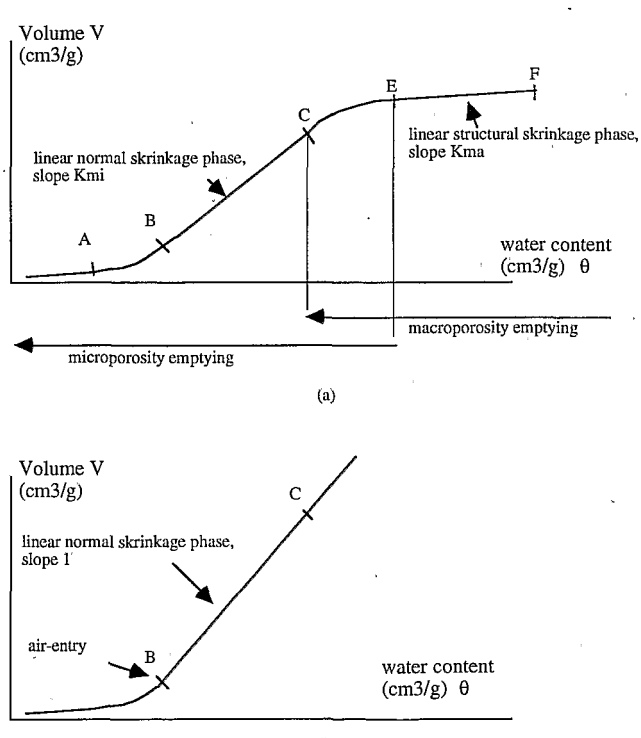

Figure 12. (a) Typical experimental shrinkage curve obtained on undisturbed soil cores and its transition points (adapted from *Braudeau* [1988a]). (b) The shrinkage curve of pure clay (adapted from *Sposito and Giraldez* [1976] and *Braudeau and Bruand* [1993]).

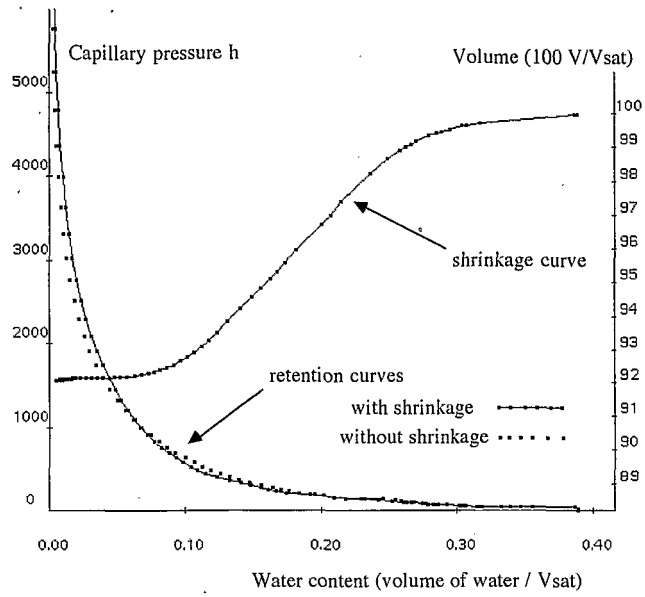

Figure 13. Deformation simulation 1. The swelling state is the one shown in Figure 6. The retention curve in drainage (without shrinkage) is identical to the drainage curve shown in Figure 11. When the presented shrinkage curve is prescribed according to scenario 1, the retention curve (with shrinkage) is modified.

Simulation 1

A first scenario consists in prescribing a given macroscopic shrinkage curve (Figure 12a) for the virtual sample, imagining any possible internal geometric reorganization of the structure. Thus ΔV_0 is known at each simulation step, ΔV_n must be zero at the particle level, and any variation of volume can be chosen on the other levels of aggregation, as long as the particles do not overlap. In the case of Figure 13, we assumed that $\Delta V_i = (1 - (i/n))\Delta V_0$.

Simulation 2

To simulate a deformation process as described by *Braudeau* [1988a,b, 1993], we consider an incomplete fragmentation, and the solid elements obtained on the last simulated level of fragmentation are microporous black boxes representing the clayey aggregates. The water content in the microporosity is denoted θ_{micro} and added to the simulated water content θ_{macro} in the macroporosity.

The simulation starts from a saturated swelling state and proceeds with successive increments Δh of the capillary pressure. First, from point F to point C of the shrinkage curve, water is drained out of the macroporosity with a variation ΔV_0 equal to $k_{\text{ma}}\Delta\theta_{\text{macro}}$ (Figure 12a) and the same assumptions are made on internal modifications ΔV_i as in simulation 1. Then, from point E to point A, the elementary behaviors of the clayey aggregates of level n are introduced into the simulation. We impose a specific shrinkage law $\Delta V_n = f(\Delta\theta_{\text{micro}})$ according to Figure 12b. These local deformations are transmitted from the internal level n to the macroscopic level 0 so that $\Delta V_0 = k_{mi}\Delta V_n$, where k_{mi} is the main parameter of the experimental curve (Figure 12a) and so that $\Delta V_0 = k_{mi}\Delta\theta_{\text{micro}} = k_{mi}\Delta\theta$ from point C to point B (when $\Delta V_n = \Delta\theta_{\text{micro}}$, cf. Figure 12b, and $\Delta\theta_{\text{micro}} = \Delta\theta$, cf. Figure 12a). At any level i, in the case of Figure 13, we assumed that $\Delta V_i = k_{mi}^{((n-i)/n)}\Delta V_n$. Water is first extracted from shrinking satu-

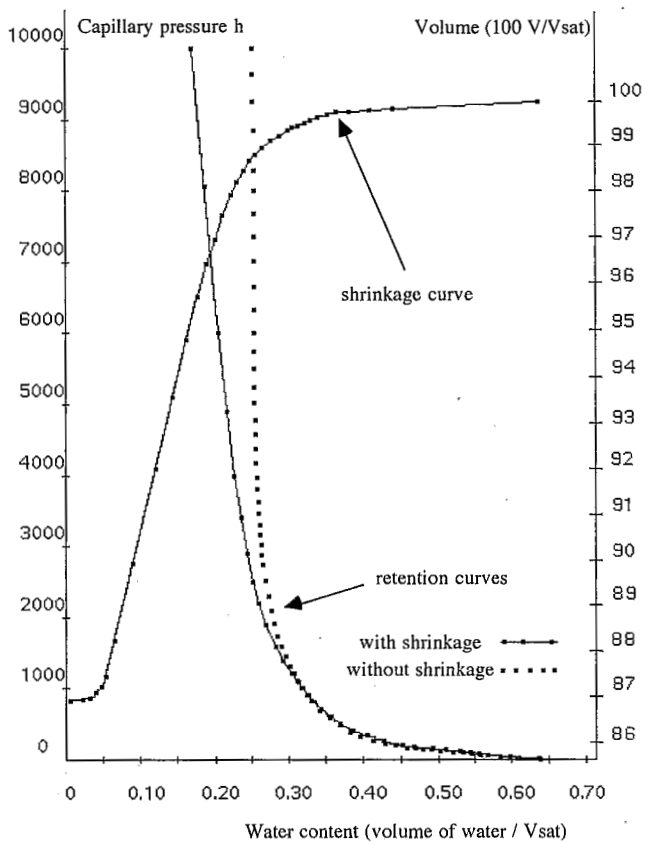

Figure 14. Deformation simulation 2. The swelling state of the structure in the saturated state is the one shown in Figure 6 (looking at Figure 6, the black solid elements represent now microporous clayey aggregates and the white channels represent the macropores only). According to scenario 2, the shrinkage process results in a modification of the retention curve associated to the macropore system (without shrinkage) to account for the micropore system (with shrinkage).

rated micropores without air entry, so that the corresponding law $h(\theta_{\text{micro}})$ must obey other physical laws in addition to that of Laplace. We assumed a quasi linear $h(\theta_{\text{micro}})$ law so that the simulation would reproduce the section E-C of the shrinkage curve (Figure 12a), where the drainage of the macroporosity is simulated and the drainage of the microporosity is calculated simultaneously.

Boivin [1990] performed retention measurements and shrinkage measurements simultaneously. He showed that the data (obtained only during the first part of the drying process, from point F to C on Figure 12a) did not fit the classical *van Genuchten* model [1980] except if the pressure was plotted against the water content in the macroporosity only. The assumption made here on the $h(\theta_{\text{micro}})$ law similarly modifies the retention curve (Figure 14).

Whatever the scenarios, the main result is a different psd for the wet and the dry states. Simulation 1 leads to pores of reduced size in the dry soil at all organization levels; the shapes of the two psds are similar (Figure 15a and 15b), because the deformation is uniformly distributed across the different levels of the structure. Simulation 2 represents the modification of the macropore system (Figure 16a and 16c) whose volume increased during drying because the internal shrinkage of clayey aggregates was greater than that of the whole soil. On the contrary, the size of the intra-aggregate micropores strongly decreased but only the uniformly reduced size of the clayey aggregates is represented (Figure 16b and 16d). Comparisons between dry and wet psds on experimental data could allow one to discriminate among the different possible assumptions used in the interpretation of the shrinkage process.

Simulation of the Conductivity Curve

Principle

The unsaturated hydraulic conductivity of the soil model $K(\theta)$ is calculated by analogy with electrical transport in a classical manner [e.g., *Fatt*, 1956; *Wise*, 1992]. Each pore has an elementary hydraulic "resistance" varying as a power law of its aperture (in a fracture of aperture r and length l, the flow is proportional to r^3/l, according to the analog of Poiseuille's law, *de Marsily* [1986]). At a given moisture content, if a pressure gradient is prescribed between two opposite sides, water flows through the subnetwork of pores filled with water and connected both to the inlet and the outlet of the sample. The sum of the local flows at each internal node of this Kirchoff network must be zero. This condition leads to a linear system to solve, imposing a precise potential at each point. The macroscopic equivalent resistance or hydraulic conductance is then derived.

First Results

It is clear that this capillary conductivity is zero as long as no continuous path of water links the two opposite sides. Hence on the random network, this is true below the percolation threshold for entering water, that is, for low and medium water content. On the fractal structure, the "belts" of large pores surrounding the thin intra-aggregate pores prevent water from flowing except in saturated soils (Figure 11b and 11c) and the

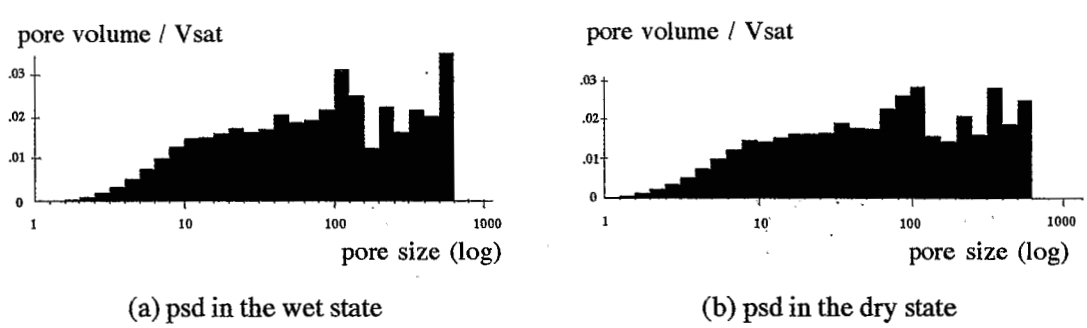

(a) psd in the wet state (b) psd in the dry state

Figure 15. Deformation simulation 1: pore size distribution (psd) (a) before and (b) after shrinkage.

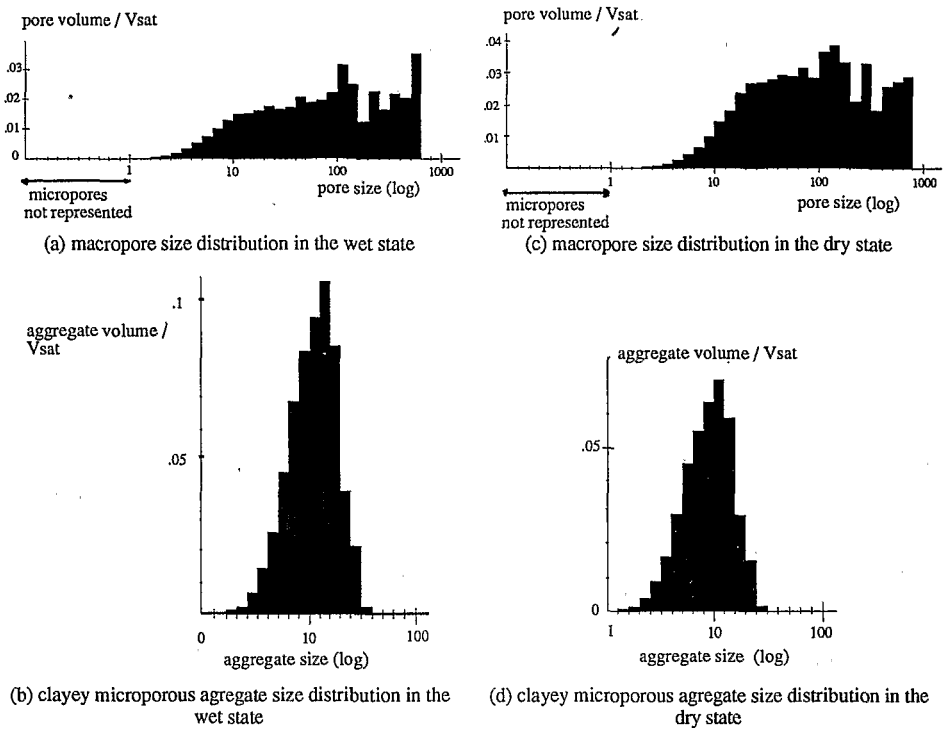

Figure 16. Deformation simulation 2: Clayey aggregate size distribution (a) before and (b) after shrinkage. Macropore size distribution (c) before and (d) after shrinkage.

conductivity rapidly drops toward zero as soon as the saturation decreases (Figure 17). Moreover, deformation emphasizes the phenomenon when the macropores enlarge during the simulation of a drying process. Although this has been observed in some soils, structured into rigorously disconnected aggregates [*Hillel*, 1982], we think that the fractal model can describe a wide range of aggregated soils where scaling laws have been observed on the pore size distribution [e.g., *Rieu and Sposito*, 1991c]. The problem is how do micropores embedded in aggregates exchange water when the larger pores are empty? We present here two attempts at answering this question, and the presented simulations have been carried out on rigid structures.

Multiple Plane Realizations

First, we tried to improve the topological structure of our constructions. It was assumed that some bridges between aggregates could exist in three-dimensional structures and we generated several plane realizations linked by transversal connections. Two random realizations of the same fragmentation process have the same number of nodes. A one-to-one correspondence was established from one node M to its closest neighbor M' in the adjacent plane (Figure 18). In order not to disrupt the spatial organization, we looked for an optimal proximity condition between two associated nodes by minimizing the sum of the distances (M, M') in the direction perpendicular to the flow. Each node was connected to three neighbors in its own plane and associated with another one in the next plane. In a two-plane realization, if two associated nodes are linked by an additional pore, four pores intersect at the

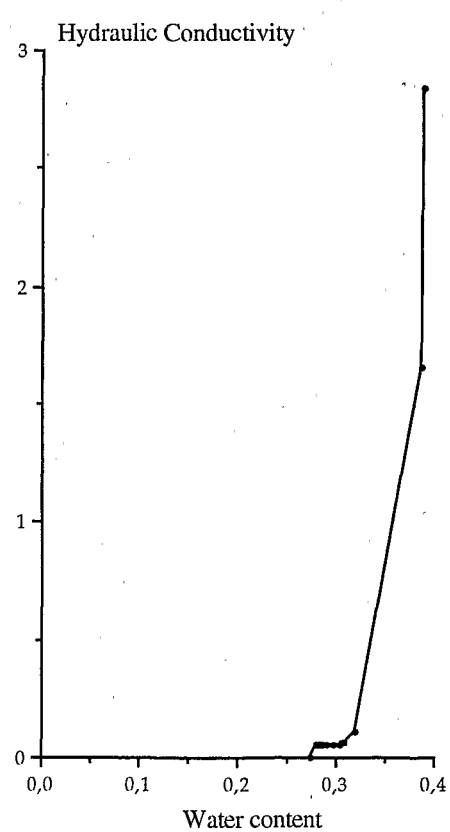

Figure 17. Conductivity curve simulated on the fractal soil structure shown in Figure 6.

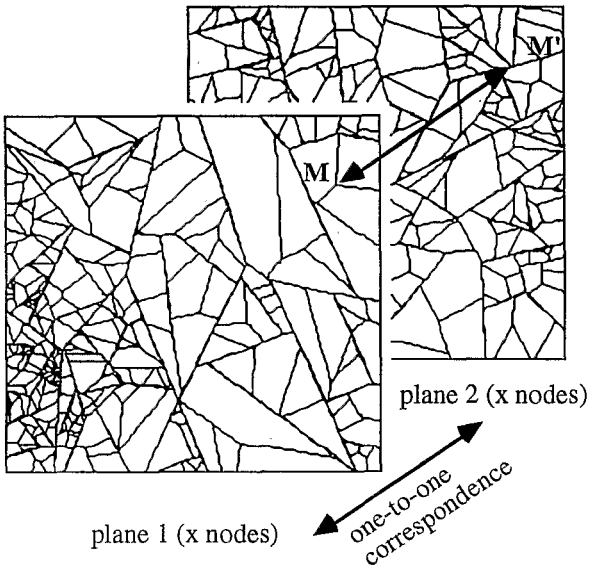

Figure 18. Transversal connections between two independent plane realizations.

same point (coordination 4); if a direct connection is established between two associated nodes, six pore intersect at the same point (coordination 6). This leads to analogs of square, or hexatriangular networks, whereas in a single plane we delt with analogs of hexagonal networks. Many variants were tested with two or more planes. In every case, a better conductivity was established and the shape of the conductivity curve is plausible (Figure 19a).

However, the larger the coordination of the pore network, the smaller the percolation threshold, and while conductivity predictions are improved, the hysteresis of the pressure curve disappears (Figure 19b). This phenomenon seems, a posteriori, easily understandable considering the imbibition phase, which was the main source of hysteresis. As soon as there is a possibility that one conducting path of water may exist between two opposite edges (the conductivity of water is nonzero above this critical water content), then other paths with the same probability in all directions of space may also exist. All the pores connected to these paths become within reach, and the size of the cluster of water-filled pores increases dramatically with a decrease in pressure. When all the pores of the medium are connected to this cluster, a perfect connectivity is established and the imbibition-retention curves matches the reference curve.

The multiplane simulation keeps exactly the same structures as in the previous sections, that is, two-dimensional structures with extrapolation of the water content in three dimensions, but it arbitrarily changes the connections of the set of pores when representing a three-dimensional connectivity in a conceptual way. The unsaturated conductivity curve seems qualitatively well simulated, but the hysteresis of the retention curve as well as the "realistic" aspect of our constructions disappear.

Anisotropic Structures

The second attempt at solving the problem of conducting paths of small pores at low water content consists in actually representing these paths. Here we simulated the formation of preferential conducting paths in a single direction denoted y.

Fractal theories generally concern self-similar structures but can also include the case of self-affine structures which are invariant, not under homothetic but affine transformations [*Falconer*, 1990]. This gave rise to the idea of creating anisotropic soil structures by replacing the previous homothetic transformations $\mathcal{H}(G, k_i)$ (Figure 20b) by affine transforma-

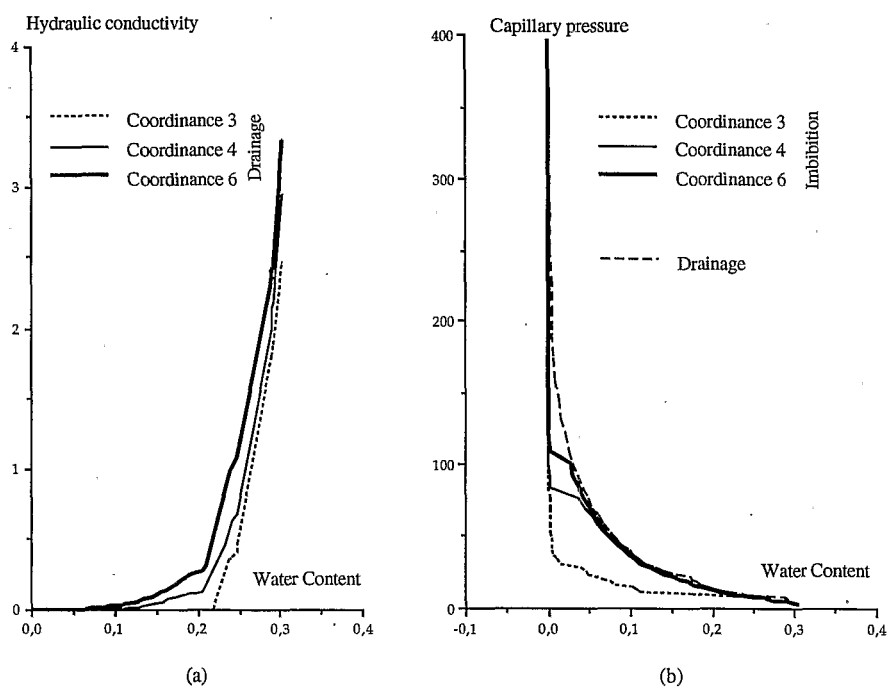

Figure 19. Multiplane realizations (two planes) of a fractal structure (same parameters as in Figure 6, but two random realizations with $n = 3$ levels only). (a) Conductivity curves simulated in drainage using different coordination numbers. (b) The hysteresis of the pressure water content relationship reduces when the coordination increases.

tions $\mathcal{A}(Gy, k_{xi})$ (Figure 20c) at each fragmentation level $i > 0$. This consists in locally reducing the polygonal zones of the structure skeleton by k_{xi} factors in only the "horizontal" direction x, which opens pores mainly in the "vertical" direction y, while a global vertical reduction is applied to the whole structure in order to conserve isotropy for the particles themselves.

This anisotropic structure could represent either a vertical plane in some settled soils, or any other direction of anisotropy linked to the soil pedogenesis. One could also imagine that our simulated plane no longer models a representative plane section of a soil, but a nonplanar three-dimensional surface going through the main joints ensuring continuous conducting paths between the soil aggregates.

Unfortunately, local overlaps may occur (Figure 20c) and make it impossible to manage this type of anisotropy. An intermediate way to proceed is to use the geometric composition of two affine transformations $\mathcal{A}(Gy, k_{xi})$ and $\mathcal{A}(Gx, k_{yi})$.

$$\text{If } k_{yi} = k_{xi}(= k_i),\ \mathcal{A}(Gy, k_{xi}) \circ \mathcal{A}(Gx, k_{yi}) = \mathcal{H}(G, k_i).$$

$$\text{If } k_{yi} = 1,\ \mathcal{A}(Gy, k_{xi}) \circ \mathcal{A}(Gx, k_{yi}) = \mathcal{A}(Gy, k_{xi}).$$

Consider an anisotropy coefficient α such that

$$1 - k_{yi} = \frac{1 - k_{xi}}{\alpha} \qquad (\alpha > 1)$$

If $\alpha = 1$, we obtain the same isotropic construction as described previously (Figure 20b). If $\alpha \to \infty$, the tendency is toward the complete anisotropic structure where overlaps may occur (Figure 20c). For the purpose of extrapolating the porosities to the three-dimensional associated sample (see appendix), we assumed a complete opening in the third direction z with $k_{zi} = k_{xi}$.

A strictly self-affine fractal is obtained when the number N of subaggregates at each iteration step is constant and the reduction ratios k_{xi}, k_{yi}, and k_{zi} are constant across all the fragmentation level i: $k_{xi} = k_x$, $k_{zi} = k_z$ and $k_{yi} = 1 - 1 - k_x/\alpha$. The theoretical fractal three-dimensional dimension D_{aff} is then the sum [*Falconer*, 1990] of each one-dimensional fractal dimension of fractal sets whose cross product results in the three-dimensional structure:

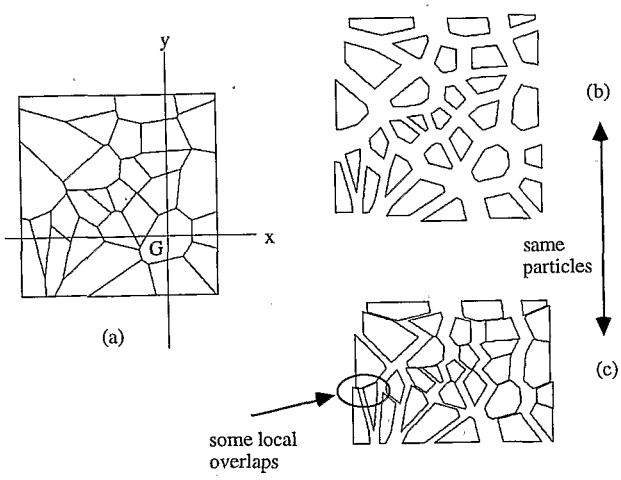

Figure 20. For the same (a) structure skeleton on one level of fragmentation, (b) isotropic and (c) anisotropic associated soil structures.

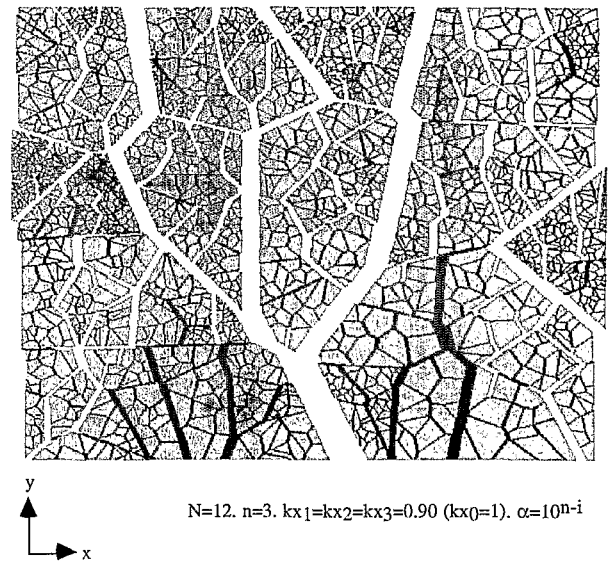

Figure 21. Anisotropic fractal soil structure. Anisotropy coefficient: $\alpha_i = \beta^{n-i}$, $\beta = 10$.

$$D_{\text{aff}} = \mathcal{D}_x + \mathcal{D}_y + \mathcal{D}_z = \log N/(\log N - 2\log(k_x) + \log N/(\log N - 2\log(k_y) + \log N/(\log N - 2\log(k_z).$$

In such self-affine fractal structures, the fitting of the simulated reference retention curve to the analytical (1) is quite good and provides good estimates D_{est} of the theoretical value of D_{aff} proposed by Falconer (on 100 random simulations where $2 < D_{\text{aff}} < 3$, with 50 simulated points (θ, h), the mean squared correlation coefficient is $R^2 = 0.98$, the mean deviation $|D_{\text{est}} - D_{\text{aff}}|$ is 0.05).

However, α cannot take large values without overlapping, and the goal of obtaining a better conductivity at low water content by reducing pore size in the direction x is not achieved. The choice of anisotropy coefficients varying with the scale makes it possible to use high anisotropy coefficients for the first fragmentation levels. Thus the biggest aggregates are drawn closer to each other and connected, while overlapping is avoided with a further decrease in anisotropy at succeeding levels. We chose an anisotropy coefficient α decreasing with an increasing level i of fragmentation: $\alpha_i = \beta^{n-i}$. Thus the greater the length scale, the larger the anisotropy, which has sometimes been reported in real observations [e.g., *Scott et al.*, 1986]. A realization of such a structure is shown in Figure 21. The hysteresis of the simulated retention curve is clear (Figure 22a). Although no theoretical result is available to determine the existence and value of a purely geometrical fractal dimension of this structure, the fitting of the intermediate reference retention curve on the analytical (1) is again quite good (Figure 22b) and provides an equivalent fractal dimension.

The simulated conductivity is only a directional conductivity in the anisotropy direction y. The water content threshold, above which the sample becomes water-conducting, decreases with increasing anisotropy (increasing α) (Figure 23), but it remains too high, since α cannot be increased ad infinitum without overlapping because of the geometrical constraints imposed by our construction. Thus this second type of simulation in our research into conducting paths at any water content was not completely successful.

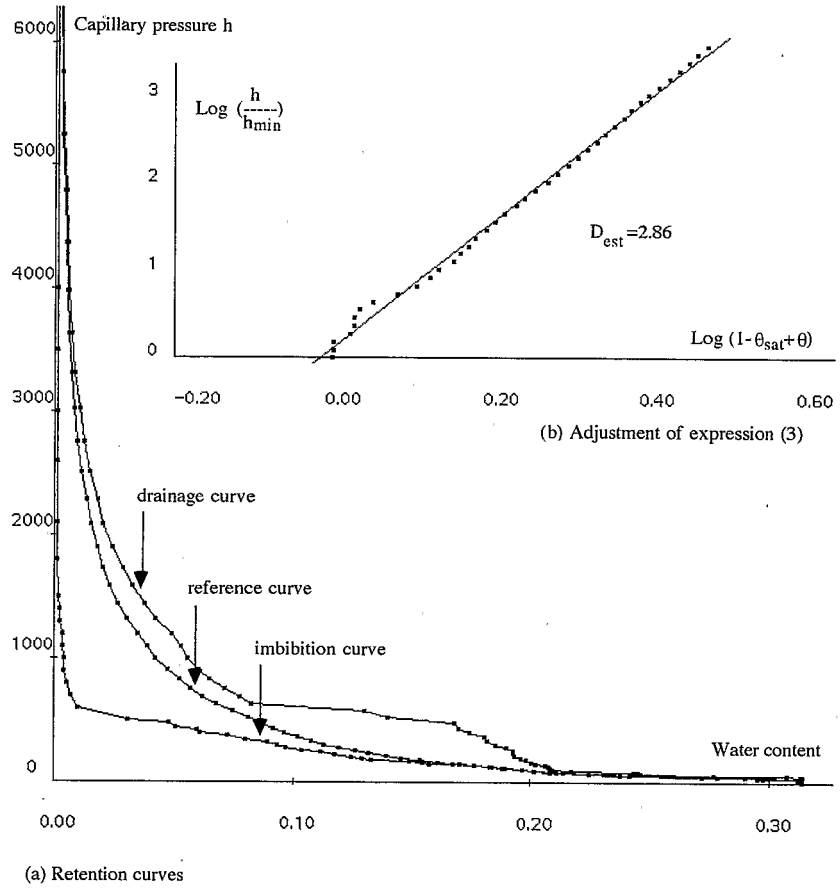

Figure 22. (a) Simulated retention curve(s) on the structure shown in Figure 21. (b) Adjustment of the reference retention curve to (3).

Discussion

These preliminary results underline the strong influence on the conductivity curve of both the topological and geometrical components of the structure. Our construction method can easily be adapted to represent different types of structure with the same pore size distribution. On the one hand, the structure model can be improved, for example, better realism will be achieved with an extension to three-dimensional realizations. On the other hand, other physical conducting principles might be introduced, considering various assumptions classically used to improve the realism of the physical flow processes, considering trapping phenomena particularly in drainage [e.g., *Ewing and Gupta*, 1993a,b; *Chatzis and Dullien*, 1982], introducing pore level cooperative invasion mechanisms especially in imbibition [whose importance has been underlined by *Lenormand et al.*, 1988; *Martys et al.*, 1991; *Koiller et al.*, 1992], and studying another type of flow along thin films of water surrounding particles at low water content [e.g., *Toledo et al.*,

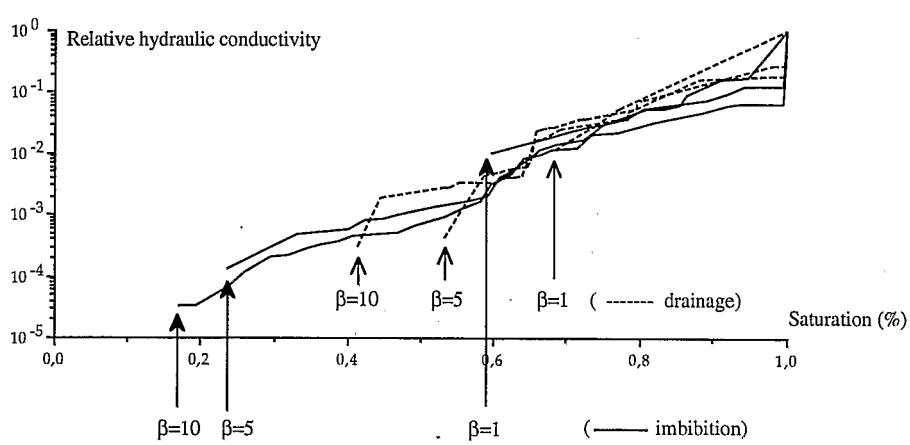

Figure 23. Conductivity curves simulated on the structure shown in Figure 21, and using variable anisotropy coefficients $\alpha_i = \beta^{n-i}$ at each level i.

1990; *Daian and Saliba*, 1991]. The effects of these mechanisms are likely to be large [*Blunt et al.*, 1992] and should be considered in further studies.

Conclusions

As a contribution to the search for deterministic links between structural and hydraulic properties of soils, this work aims to provide a new geometric approach for modeling soil structures. It is based on observations of the organization of many soils structured on hierarchical levels of particle aggregates which may deform with variations in water content. A method for constructing virtual soils is proposed, using random Voronoï tesselations to fragment a representative two-dimensional area into irregular zones, extending these tesselations to embedded levels of fragmentation, and then, creating rigid or deformable porous structures by means of homothetic transformations at each level. A realistic representation of the spatial organization of the pore space, which is linked to the particle aggregation state, imposes strong coherence conditions on the structure model.

The method makes it possible to represent theoretical soil structure models already established in soil science. A fractal model of aggregated soils is thus reproduced and generalized to the case of a random and irregular aggregate morphology closer to reality. The water retention curve which is associated by a simple capillary model with the simulated pore size distribution fits the same analytic expression as the one calculated on the regular deterministic model. Furthermore, it is now possible to take into account deformability as additional information on soil structures. To reproduce shrinkage curves, obtained at the sample macroscopic scale, several scenarios may be developed to represent internal modifications of aggregate volumes at each organization level resulting in pore size distribution variations due to the swelling state of the soil. One particular soil model assumes a specific behavior for micropores included in clayey microaggregates.

On these virtual structures, classical methods mainly used on random pore networks can be applied to simulate their hydraulic properties. By simulating simple invasion percolation processes for both air and water on the interconnected network, one can represent the primary and secondary hysteretic loops of the retention curve. The fractal analytic expression of the retention curve is still well fitted by the drainage curve. The value of the hydraulic conductivity is strongly affected by the structure model: it would be zero below complete saturation for the studied fractal model representing soils structured into strictly disconnected aggregates. A more usual shape of the conductivity curve is obtained when the model is extended to represent aggregate interconnections either by imagined transversal links between plane realizations or the generation of anisotropic fractal models that lead to preferential flows in a given direction. This shows the robustness of the notion of fractal pore size distribution but also the necessity to clarify its spatial distribution in order to realistically predict hydraulic conductivity.

Our main contribution is to propose a methodology for taking into account the spatial structuring of soils in the field of pore network modeling, including for the first time, geometrical modifications due to varying water content. We started from very simple hypotheses, both on the structure model and on the physical water processes involved, then we progressively increased the level of complexity and realism. Further studies will be made to investigate a wider range of hypotheses, and this can be done with the same construction algorithms and simulation principles.

Appendix: Calculation of Pore Volumes From Plane Representations

We can measure on the simulated soil structures the surface $S(p)$ of a pore p (normalized by the surface of the whole simulated plane region P_0). The corresponding volumetric water content $V(p)$ of this pore would be equal to $S(p)$ if the fractures had an infinite extension in the third dimension, which is not simulated. However, if we consider an identical fragmentation process in each space direction,

$$V(p, i) = S(p, i)^{*}\mathrm{coeff}(i) \tag{A1}$$

where coeff(i) is a correction coefficient at each fragmentation level i, $i > 0$:

If we consider an isotropic fragmentation process,

$$\mathrm{coeff}(i) = \frac{1 - k_i^3}{1 - k_i^2} \prod_{j=0}^{i-1} k_j \tag{A2}$$

Knowing the relationship between the represented surface $SA(i)$ of all aggregates of level i and the extrapolated volume $VA(i)$ from (1) and (2) ($SA(i) = \Pi_{j=0}^{i} k_j^2$ and $VA(i) = \Pi_{j=0}^{i} k_j^3$), we calculated the ratio between the represented surface $SP(i)$ of all aggregates of level i and the extrapolated volume $VP(i)$ as follows:

$$SP(i) = SA(i-1) - SA(i) = \prod_{j=0}^{i-1} k_j^2 - \prod_{j=0}^{i} k_j^2$$

$$= (1 - k_i^2) \prod_{j=0}^{i-1} k_j^2$$

and

$$VP(i) = VA(i-1) - VA(i) = \prod_{j=0}^{i-1} k_j^3 - \prod_{j=0}^{i} k_j^3$$

$$= (1 - k_i^3) \prod_{j=0}^{i-1} k_j^3$$

The ratio coeff(i) = $VP(i)/SP(i)$ is used to calculate the volume of each pore p of level i from its plane surface.

In the last case of anisotropic structures (k_{xi}, k_{yi}, $k_{zi} = k_{xi}$), the correction coefficient can be calculated in the same manner for a whole fragmentation level:

$$\mathrm{coeff}(i) = \frac{1 - k_{xi}k_{yi}k_{zi}}{1 - k_{xi}k_{yi}} \prod_{j=0}^{i-1} k_{zj} = \frac{1 - k_{xi}^2 k_{yi}}{1 - k_{xi}k_{yi}} \prod_{j=0}^{i-1} k_{xj} \tag{A3}$$

and this mean value is applied to each individual correction of a given pore p.

Notation

P a polygonal zone in the Voronoï fragmentation process.

i any fragmentation level.
n number of fragmentation levels.
P_{ij} a polygonal zone labeled j, created at the ith fragmentation level.
$\mathcal{H}(G, k)$ homothetic transformation with center G and ratio k.
G_{ij} center of gravity of the polygon P_{ij}.
k_i ratio of the transformation $\mathcal{H}(G_{ij}, k_i)$ applied at level i to any polygon P_{ij} to create an aggregate A_{ij}.
A_{ij} shrinked polygonal zone representing an aggregate of level i.
N constant number of fragmentation zones daughters in the fractal case.
k constant homothetic ratio in the fractal case.
$\mathcal{D}$ theoretical fractal dimension of a self-similar fractal model.
$\mathcal{D}_2$ fractal dimension calculated on a bidimensional virtual structure.
$\mathcal{D}_3$ fractal dimension calculated on a virtual structure when it is extrapolated to a tridimensional structure as explained in text.
D_{def} fractal dimension calculated on a virtual fractal structure (it equals $\mathcal{D}_3$ in the presented examples).
D_{est} (resp. D'_{est}) fractal dimension estimated from the fit of retention data to theoretical analytical (3) (or (4)).
θ, (resp. θ_{sat}) water content (or value in a water-saturated soil sample).
h (resp. $h_{\min}$) capillary pressure (or capillary pressure at air entry).
V (resp. V_{sat}) volume (or value in a water-saturated soil sample).
K (resp. K_{sat}) hydraulic conductivity (or value in a water-saturated soil sample).
A, B, C, E, F transition points of a shrinkage curve [*Braudeau*, 1988a].
$\theta_{\text{macro}}, \theta_{\text{micro}}$ water content in the macroporosity, in the microporosity.
$k_{\text{ma}}, k_{\text{mi}}$ slopes of the linear parts of a shrinkage curve (in scenario 2, they explain, respectively, the shrinkage of the soil macroporosity and microporosity).
(s) any swelling state of a deforming structure.
$k_i(s)$ variable value of the homothetic ratio k_i defining a swelling state (s).
$\lambda_i(s)$ product of homothetic ratios: $\lambda_i(s) = \Pi_{j=0}^{i} (k_j(s))$.
ΔV_i variation of the partial volume V_i occupied by all the aggregates of level i between two successive swelling states (s) and (s').
$\mathcal{A}(Gx, k)$ affine transformation with ratio k, perpendicular to the line Gx.
D_{aff} fractal dimension of a self-affine fractal structure.
α anisotropy coefficient.
β $\alpha = \beta^{n-i}$ when α varies with the fragmentation level i.

References

Ahl, C., and J. Niemeyer, The fractal dimension of the pore volume inside soils, *Z. Planzenernähr. Bodenk.*, *152*, 457–458, 1989a.

Ahl, C., and J. Niemeyer, Fractal geometric objects in the soil, *Mitt. Deutsch. Bodenk.*, *59*(1), 93–98, 1989b.

Arya, L. M., and J. F. Paris, A physicoempirical model to predict the soil moisture characteristic from particle-size distribution and bulk density data, *Soil Sci. Soc. Am. J.*, *45*, 1023–1030, 1981.

Bartoli, F., R. Philippy, M. Doirisse, S. Niquet, and M. Dubuit, Silty and sandy soil structure and self-similarity: The fractal approach, *J. Soil Sci.*, *42*, 167–185, 1991.

Billaux, D., Hydrogéologie des milieux fracturés, Géométrie, connectivité et comportement hydraulique, Document du BRGM 186, Thèse, école des Mines de Paris, Paris, 1990.

Billotte, J., Modélisation de milieux poreux pour la détermination des paramètres nécessaires au calcul d'écoulements alternés, Thèse, Ecole des Mines de Paris, Paris, 1986.

Blunt, M., M. J. King, and H. Scher, Simulation and theory of two-phase flow in porous media, *Phys., Rev. A.*, *46*(12), 7680–7699, 1992.

Boivin, P., Caractérisation physique des sols sulfatés acides de la vallée de Katoure (Basse Casamance), *Thèse, Université Paris*, *6*, Paris, 1990.

Braudeau, E., Equation généralisée des courbes de retrait d'échantillons de sols structurés, *C. R. Acad. Sci. Sér. 2*, *307*, 1731–1734, 1988a.

Braudeau, E., Essai de caractérisation quantitative de l'état structural d'un sol basé sur l'étude de la courbe de retrait, *C. R. Acad. Sci. Sér. 2*, *307*, 1933–1936, 1988b.

Braudeau, E., and A. Bruand, Détermination de la courbe de retrait de la phase argileuse à partir de la courbe de retrait établie sur des échantillons de sol non remanié; Application à une séquence de sols de Côte d'Ivoire, *C. R. Acad. Sci. Sér. 2*, *316*, 685–692, 1993.

Braudeau, E., and P. Boivin, Transient determination of shrinkage curve for undisturbed soil samples: A standardized experimental method, in *Clay Swelling and Expansive Soils*, edited by P. Baveye and M. B. McBride, Kluwer Academic, Norwell, Mass., (in press), 1995.

Brooks, R. H., and A. T. Corey, Hydraulic properties of porous media, in *Hydrology Paper 3*, Colo. State Univ., Fort Collins, 1964.

Cacas, M. C., E. Ledoux, G. de Marsily, A. Barbreau, E. Durand, B. Feuga, and P. Peaucederf, Modelling fracture flow with discrete fracture network: Calibration and validation, 1, The flow model, *Water Resour. Res.*, *26*(3), 479–489, 1990a.

Cacas, M. C., E. Ledoux, G. de Marsily, A. Barbreau, P. Calmels, B. Gaillard, and R. Margrita, Modelling fracture flow with discrete fracture network: Calibration and validation, 2, The transport model, *Water Resour. Res.*, *26*(3), 491–500, 1990b.

Charlaix, E., E. Guyon, and S. Roux, Permeability of random array of fractures of widely varying apertures, *Transp. Porous Media*, *2*, 31–43, 1987.

Chatzis, I., and F. A. L. Dullien, Modelling pore structure by 2-D and 3-D networks with application to sandstones, *J. Can. Pet., Techol.*, *16*, 97–108, 1977.

Chatzis, I., and F. A. L. Dullien, Mise en oeuvre de la théorie de la percolation pour modéliser le drainage des milieux poreux et la perméabilité relative au liquide non mouillant injecté, *Rev. Inst. Fr. Pét.*, *37*(2)2, 183–205, 1982.

Daian, J. F., and J. Saliba, Détermination d'un réseau aléatoire de pores pour modéliser la sorption et la migration d'humidité dans un mortier de ciment, *Int. J. Heat Mass Transfer*, *34*(8), 2081–2096, 1991.

de Gennes, P. G., Partial filling of a fractal structure by a wetting fluid, in *Physics of Disordered Materials*, P. M. Adler et al., pp. 227–241, Plenum, New York, 1985.

Delannay, R., J. F. Thovert, and P. M. Adler, Fractals et milieux poreux, *Rev. Int. Syst.*, *3*, 4, 1989.

Diaz, C. E., I. Chatzis, and F. A. L. Dullien, Simulation of capillary pressure curves using bond correlated site percolation on a simple cubic network, *Transp. Porous Media*, *2*, 215–240, 1987.

di Pietro, L. B., A. Melayah, and S. Zaleski, Modeling water infiltration in unsaturated porous media by interacting lattice gas-cellular automata, *Water Resour. Res.*, *30*(10), 2785–2792, 1994.

Ewing, R., and S. C. Gupta, Modeling percolation properties of random media using a domain network, *Water Resour. Res.*, *29*(9), 3169–3178, 1993a.

Ewing, R., and S. C. Gupta, Percolation and permeability in partially structured networks, *Water Resour. Res.*, *29*(9), 3179–3188, 1993b.

Falconer, K., *Fractal Geometry*, John Wiley, New York, 1990.

Fatt, I., The network model of porous media, I, II, III, *Trans. Am. Inst. Min. Metall. Pet. Eng.*, *207*, 144–177, 1956.
Friesen, W. I., and R. J. Mikula, Fractal dimensions of coal particles, *J. Colloid Interface Sci.*, *120*, 263–271, 1987.
Gerke, H. H., and M. T. van Genuchten, A dual porosity model for simulating the preferential movement of water and solutes in structured porous media, *Water Resour. Res.*, *29*, 305–319, 1993.
Ghilardi, P., A. Kaikai, and G. Menduni, Self-similar heterogeneity in granular porous media at the representative elementary volume scale, *Water Resour. Res.*, *29*(4), 1205–1215, 1993.
Golden, J. M., Percolation theory and models of unsaturated porous media, *Water Resour. Res.*, *16*, 201–209, 1980.
Green, P. J., and R. Sibson, Computing dirichlet tessellations in the plane, *Comput. J.*, *21*(2), 168–173, 1977.
Haines, W. B., The volume-changes associated with variations of water content in soil, *Soil J. Agric. Sci.*, *1*(3), 296–310, 1923.
Haverkampf, R., and J. Y. Parlange, Predicting the water retention curve from particle-size distribution: Sandy soils without organic matter, *Soil Sci.*, *142*, 325–339, 1986.
Jullien, R., and R. Botet, Aggregation and Fractal Aggregates, *World Scientific*, Singapore, 1986.
Katz, A. J., and A. H. Thompson, Fractal sandstone pores: Implication for conductivity and pore formation, *Phys. Rev. Lett.*, *54*(12), 1325–1328, 1985.
Koiller, B., H. Ji, and M. O. Robbins, Fluid wetting properties and the invasion of square networks, *Phys. Rev. B Condens. Matter*, *45*(14), 7762–7767, 1992.
Lenormand, R., and C. Zarcone, Description des mécanismes d'imbibition dans un réseau de capillaires, *C. R. Acad. Sci. Sér. 2*, *297*, 393–396, 1983.
Lenormand, R., and C. Zarcone, Invasion percolation in an etched network: Measurement of a fractal dimension, *Phys. Rev. Lett.*, *54*(20), 2226–2229, 1985.
Lenormand, R., E. Touboul, and C. Zarcone, Numerical models and experiments on immiscible displacements in porous media, *J. Fluid Mech.*, *189*, 165–187, 1988.
Marshall, T. J., A relation between permeability and size distribution of pores, *J. Soil Sci.*, *9*(1), 1–8, 1958.
de Marsily, G., *Quantitative Hydrogeology: Groundwater Hydrology for Engineers*, Academic San Diego, Calif., 1986.
Martys, N., M. Cieplak, and M. O. Robbins, Critical phenomena in fluid invasion of porous media, *Phys. Rev. Lett.*, *66*(8), 1058–1061, 1991.
McGarry, D., and K. W. J. Malafant, The analysis of volume change in unconfined units of soil, *Soil Sci. Soc. Am. J.*, *51*, 290–297, 1987.
Mualem, Y., A conceptual model of hysteresis, *Water Resour. Res.*, *10*(3), 514–520, 1974.
Mualem, Y., Hysteretical models for prediction of the hydraulic conductivity of unsaturated porous media, *Water Resour. Res.*, *12*(6), 1248–1254, 1976.
Nordqvist, A. W., Y. W. Tsang, C. F. Tsang, B. Dverstorp, and J. Andersson, A variable aperture fracture network model for flow and transport in fractured rocks, *Water Resour. Res.*, *28*(6), 1703–1713, 1992.
Oades, J. M., and A. G. Warters, Aggregate hierarchy in soils, *Aust. J. Soil Res.*, *29*, 815–828, 1991.
Othmer, H., B. Diekkrüger, and M. Kutilek, Bimodal porosity and unsaturated hydraulic conductivity, *Soil Sci.*, *152*(3), 139–150, 1991.
Perrier, E., Structure géométrique et fonctionnement hydrique des sols, Simulations exploratoires, Thèse, Université Paris, VI, Paris, 1994.
Pfeifer, P., and D. Avnir, I. Fractal theory of heterogeneous surfaces, *J. Chem. Phys.*, *79*(7), 3558–3565, 1983.
Rieu, M., and G. Sposito, Fractal fragmentation, soil porosity, and soil water properties, I, Theory, *Soil Sci. Soc. Am. J.*, *55*, 1231–1238, 1991a.
Rieu, M., and G. Sposito, Fractal fragmentation, soil porosity, and soil water properties, II, Applications, *Soil Sci. Soc. Am. J.*, *55*, 1239–1244, 1991b.
Rieu, M., and G. Sposito, Relation pression capillaire-teneur en eau dans les milieux poreux fragmentés et identification du caractère fractal de la structure des sols, *C. R. Acad. Sci. Ser. 2*, *312*, 1483–1489, 1991c.
Sposito, G., and J. V. Giraldez, Thermodynamic stability and the law of corresponding states in swelling soils, *Soil Sci. Soc. Am. J.*, *40*, 352–358, 1976.
Thirriot, C., Déplacement capillaire de fluides non miscibles dans un réseau de forme hexagonale, *C. R. Acad. Sci. Ser. 2*, *293*, 873–876, 1981.
Thirriot, C., Rusticité ou sophistication des modèles capillaires pour l'explication de l'hystérésis en milieu poreux, *Bull. GFHN*, *11*, 57–81, 1982.
Toledo, P. G., R. A. Novy, H. T. Davis, and L. E. Scriven, Hydraulic conductivity of porous media at low water content, *Soil Sci. Soc. Am. J.*, *54*, 673–679, 1990.
Tyler, S. W., and S. W. Wheatcraft, Application of fractal mathematics to soil water retention estimation, *Soil Sci. Soc. Am. J.*, *53*, 987–996, 1989.
Tyler, S. W., and S. W. Wheatcraft, Fractal processes in soil water retention, *Water Resour. Res.*, *26*, 1047–1054, 1990.
Tyler, S. W., and S. W. Wheatcraft, Fractal scaling of soil particle-size distributions: Analysis and limitations, *Soil Sci. Soc. Am. J.*, *56*, 362–369, 1992.
van Genuchten, M. T., A closed form equation for predicting the hydraulic conductivity of unsaturated soils, *Soil Sci. Soc. Am. J.*, *44*, 892–898, 1980.
Wilkinson, D., Percolation model of immiscible displacement in the presence of buoyancy forces, *Phys. Rev. A.*, *30*(1), 520–529, 1984.
Wilkinson, D., Percolation effects in immiscible displacement, *Phys. Rev. A.*, *34*(2), 1380–1391, 1986.
Wise, W. R., A new insight on pore structure and permeability, *Water Resour. Res.*, *28*(1), 189–198, 1992.
Winterfeld, P. H., Percolation and conduction phenomena in disordered composite media, Ph.D. thesis, Univ. of Minn., Minneapolis, 1981.
Young, I. M., and J. W. Crawford, The fractal structure of soil aggregates: Its measurement and interpretation, *J. Soil Sci.*, *42*, 187–192, 1991.
Zhou, D., and E. H. Stenby, Interpretation of capillary pressure curves using invasion percolation theory, *Transp. Porous Media*, *11*, 17–31, 1993.

C. Mullon, M. Rieu, and E. Perrier, LIA ORSTOM, 32, avenue Henri Varagnat, F-93143 Bondy Cedex, France. (e-mail: mullon@bondy.orstom.fr; rieu@paris.orstom.fr; perrier@bondy.orstom.fr)
G. de Marsily, Laboratoire de Géologie Appliqueé, Université Pierre et Marie Curie, Paris, France. (e-mail: gdm@ccr.jussieu.fr)

(Received January 4, 1995; revised July 14, 1995; accepted July 21, 1995.)